s c c h
software competence center
hagenberg

FUZZY.LOGIC.LAB.LINZ

Advances in Knowledge-Based Technologies

Proceedings of the Master and PhD Seminar Summer term 2008, part 1

Softwarepark Hagenberg
SCCH, Room 0/2
April 22, 2008

Software Competence Center Hagenberg
Softwarepark 21
A-4232 Hagenberg
Tel. +43 7236 3343 800
Fax +43 7236 3343 888
www.scch.at

Fuzzy Logic Laboratorium Linz
Softwarepark 21
A-4232 Hagenberg
Tel. +43 7236 3343 431
Fax +43 7236 3343 434
www.flll.jku.at

Program

13:30–15:00 Session 1 ***(Chair: Bernhard Moser)***

13:30 Leila Muresan:
New results in microarray image analysis at single molecule level

14:00 Alfredo Lopez:
Cardiac 4D image sequence registration using bridging points

14:30 Balasubramaniam Jayaram:
(S, N)- and R-implications: a state-of-the-art survey

New results in microarray image analysis at single molecule level

L. Muresan, E.P Klement[1], J. Jacak, G. Schütz[1,2], and J. Hesse[3]

[1] Department of Knowledge-based Mathematical Systems, Johannes Kepler University, Linz,
[2] Biophysics Institute, Johannes Kepler University, Linz,
[3] Upper Austrian Research. *

Abstract. In this work we present the analysis of high resolution microarray images obtained via the *Nanoreader* scanning system. *Nanoreader* via fast, high resolution and highly sensitive imaging, allows the detection of single molecule signals on the microarray slide. Through this system one gains a better understanding of the sample, even at very low concentration, by ignoring background and dye effects.
The novel technique generates the need for a new kind of analysis for the microarray image data, both for detection of signal and estimation of cDNA concentration. Detection of single molecules is performed via shrinkage of undecimated wavelet coefficients and using the positions of the single molecules, an estimation of the signal concentration is performed, based on mixture models. Two alternatives are considered in order to solve the parameter estimation task: a fast method of moments, (MOM) and a maximum likelihood based on Expectation-Maximization (EM) approach. The performance of the two approaches is discussed and finally, results of experiments on simulations and real data are provided.

* This work was supported by the GEN-AU program of the Austrian Federal Ministry of Education, Science and Culture.

CARDIAC 4D IMAGE SEQUENCE REGISTRATION USING BRIDGING POINTS

Alfredo Lopez[1,2], Karl D. Fritscher[2], Thomas Trieb[3], Rainer Schubert[2] and Julian Mattes[1]

Abstract

In this paper we present a new approach for the registration of two cardiac 4D image sequences. In a first step we establish a temporal association between the sequences. For one (or two) selected pair(s) of associated points in time of both sequences, which we call the bridging points in time, we allow the use of additional information such as the semi-automatic segmentation of the investigated structure. We establish the 3D inter-subject registration for each other pair of associated points in time exploiting (1) the inter-subject registration for the bridging pair of points in time, (2) the intra-subject motion calculation in both sequences between the currently considered points in time and the bridging pair, and (3) the concatenation of the obtained transformations. We formulate a cost functional integrating the similarity measures comparing the images of the bridging pair(s) of points in time and of the current pair of points in time, respectively. We evaluated our algorithm on 8 healthy volunteers leading to 28 inter-subject combinations and we analyze the behavior for different parameter settings weighting differently the involved pairs of points in time. The approach based on the bridging pairs outperforms a direct 3D registration of corresponding points in time, in particular in the right ventricle we gain up to 33% in registration accuracy. Starting with a cost functional taking into account the similarity at the first bridging point in time, the results improve stepwise by integrating, additionally, first, information from the current pair of points in time and secondly, from a second bridging point in time. Finally, we show an example visualizing, for different pairs of initial points in time, a comparison of the motion fields of two subjects.

1. Introduction

The need to compare the motion of anatomical structures belonging to different individuals or their shape at different selected corresponding points in time may occur in very different situations when studying kinetic processes of medical or biological objects [15]. For instance, this comparison is necessary to see how the motion of a healthy structure differs from the motion of the same kind of structure but in a pathological state [9]. If the considered anatomical structure is the heart, the comparison allows to investigate the shape variation across subjects at the initial points of the seven different phases of the cardiac cycle [8], to compare the motion fields starting from these initial points (cf., Fig. 6), and to correlate shape differences to specific characteristics of the motion occurring in the considered phase. For different heart diseases, for instance myocarditis, differences in the motion of the heart compared to healthy subjects can be observed. However, without a quantitative comparison of the motion as described above a precise characterization of these differences is not possible. In

[1]Biomedical Data Analysis Group, KBT, Software Competence Center Hagenberg, Austria.{Alfredo.Lopez, Julian.Mattes}@scch.at, www.scch.at

[2]Institute for Biomedical Image Analysis, University for Health Sciences, Medical Informatics and Technology, Austria

[3]Department of Diagnostic Radiology, Innsbruck Medical University, Austria

particular, a quantitative comparison would be helpful for the assessment of the evolution of the disease when comparing the motion of the heart of the same patient at different stages of the disease. Another task is the correction of motion artifacts [21] where the composed motion of an object moving by itself and moved by its moving environment shall be compared only with the motion of the object itself (for instance, in case of respiratory artifacts when considering cardiac motion). This correction can be based on a statistical representation of the motion, in particular on a *4D* or *motion atlas* [3, 17, 13].

When dealing with sequences of 3D (or 2D) images a *4D* (or 3D, respectively) *registration* of the image sequences is essential for the local comparison of motion [2] or the analysis of shape variation at selected points in time (e.g., the initial points of the different phases of the cardiac cycle mentioned above). 4D registration means to register not only 3D images of a time sequence but to register two different time sequences as a whole, called a "spatio-temporal alignment" [2, 14]. It implies a temporal alignment of the sequences as well as a spatial alignment. The latter mapping allows a direct local comparison of the (previously calculated) motion at anatomically corresponding points for the two investigated subjects (see Fig. 6). Additionally, typical models for the analysis of shape variation [4, 5] require the knowledge about inter-subject correspondence as provided by this alignment. 4D registration has also been used to compare sequences acquired with different modalities [23], for instance gated cardiac SPECT images with MR images [6, 1]. For building statistical motion representations [3, 17] Peperides et al. [14] proposed a spatio-temporal inter-sequence registration in which the (global and local) spatial transformation is the same for all points in time. A more detailed description of the related work can be found in Lopez et al. [10].

In this paper we consider the spatio-temporal alignment of the cardiac cycle where the spatial component may be different for each point in time. After a linear temporal association, we focus on the individual spatial 3D inter-subject registration for each pair of associated points in time. For a given pair of points in time we use 4D information by exploiting the consideration that the spatial transformation relating the two subjects at this pair of points in time is also determined by the spatial transformation for any other pair of points in time together with the intra-subject transformation relating the considered pairs of points in time (c.f., Fig. 2). Our approach uses intra-subject and inter-subject free-form registration. In the next subsection we detail some aspects of the related work mentioned above and delimit it from the work presented in this paper. A precise problem formulation is provided in Section 2. together with the presentation of the registration framework for intra- and inter-sequence analysis used in this paper. We describe our new approach in Section 3.We present our results in Section 4. before discussing them and concluding in Section 5.

2. Problem Formulation and Registration Framework

In contrast to purely spatial registration, usually, a natural condition should be imposed for spatio-temporal registration, where we aim to align two different image sequences. If $(\vec{x}, t)$, with $\vec{x} \in \mathbb{R}^d, t \in \mathbb{R}$, where d is the dimension of the space (in our case $d = 3$), denotes a point $\vec{x}$ in the image space at time t, the transformation $T_{s.t.} : \mathbb{R}^d \times \mathbb{R} \rightarrow \mathbb{R}^d \times \mathbb{R}$ between image sequences should satisfy the equation

$$T_{s.t.}(\vec{x}, t) = (T_{spat}(\vec{x}, t), T_{temp}(t)), \tag{1}$$

where T_{temp} is a monotonous increasing function and where $T_{spat}(\cdot, t)$ maps the image space onto itself. This formulation of our 4D registration problem ensures that different regions of an image stack in one sequence will be mapped to a single stack in the other sequence. The spatio-temporal

transform used in this paper differs from the one presented in (Perperidis et al. 2005) [14] where its spatial component depends uniquely on the spatial argument $\vec{x}$ and hence the same spatial transform is applied for each point in time.

If we consider a fixed point in time t and a given associated point in time $T_{temp}(t)$ the calculation of $T_{spat}(\cdot, t)$ may be achieved using purely spatial inter-patient registration. In our approach we use spatial registration also for intra-patient motion estimation. The problem of *spatial registration* is usually formulated as an optimization problem: Given a *source* image I defined over a domain $\Omega_I \subseteq \mathbb{R}^3$ and a *target* image J defined over a domain $\Omega_J \subseteq \mathbb{R}^3$ *registering* I to J consist of finding a parametric mapping $T(\cdot; \mathbf{p}^*) : \Omega_J \rightarrow \Omega_I$ within a certain class of transforms (called *transformation model*) such that its associated parameter $\mathbf{p}^*$ minimizes a certain cost functional $C(\mathbf{p}) = -S(\mathbf{p}) + \lambda R(\mathbf{p})$, i.e.

$$\mathbf{p}^* = \arg\min_{\mathbf{p} \in P} -S(\mathbf{p}) + \lambda R(\mathbf{p}). \tag{2}$$

The mapping $T(\mathbf{p}^*)$ leads (together with a subsequent gray value interpolation procedure) to a transformed source image [22]. Hence, we call the source image I also *moving* image and, correspondingly, we call the target image J *fixed* image. The functional C is composed by a similarity term $S(\mathbf{p})$ which measures how well the transformed moving image resembles the fixed image J and a *regularization* term $R(\mathbf{p})$ ensuring the smoothness of the transformation. The regularization parameter $\lambda \geq 0$ controls the trade-off between these two terms.

A similarity measure and a transformation model which have been successfully used for intra- and inter-subject registration [14] are the normalized mutual information (NMI) according to Studholme et al. [19], and tri-linear B-Splines [18]. The latter is implemented in the Insight Segmentation and Registration Toolkit (ITK) [22] using a B-spline interpolation kernel. We set the control points of the B-splines in a multi-resolution scheme. Equally, we used the ITK implementation for calculating the entropies [11] involved in the NMI measure and the L-BFGS-B minimization package as suggested in (Mattes et al. 2003) [11] and implemented in ITK. As regularization term we implemented the second order stabilizer [20]. For intra-subject registration of a given reference point in time to any other point in time we register the reference image stepwise to each successive image until the desired point in time is reached by initializing each registration process with the transformation resulting from the previous step. In our 4D analysis approach, presented in the next section, we used these components as well for intra-subject registration as well as for inter-subject registration.

3. Our Approach for 3D Registration Using 4D Information

3.1. Motivation

The images taken at comparable points in time of time sequences of different subjects may represent strong differences as well in the anatomy of the considered structure as well in the acquisition quality. Fig. 1(a,b) shows for each of two healthy volunteers (see Section 4.1.) a 2D slice of the respective 3D image of the heart obtained at the moment of the R-wave (the *first* point in time of our image sequences). In the image in Fig. 1(a) a structure not belonging to the right ventricle is visible close to the right ventricle which appears in a different way in Fig. 1(b). For this reason a strong mismatch occurs after normalized mutual information (NMI) based B-Spline registration as shown in Fig. 1(c). However, if we *mask* the image after a segmentation of the endocardial surface (the values outside this surface are set to gray-level 0 by the masking, the other values are not changed) we obtain a good result with the same registration technique also in the critical regions of the right ventricle (Fig. 1(d)).

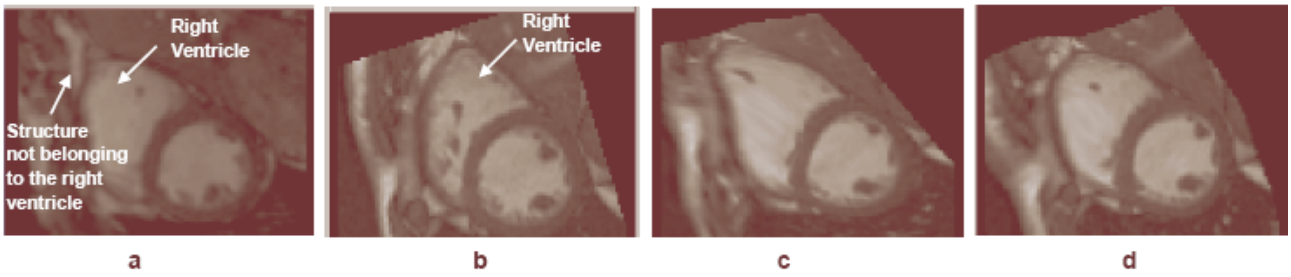

Figure 1. Normalized mutual information (NMI) based 3D inter-subject registration of the hearts for two subjects at the moment of the R-wave (for the purpose of obtaining images representing the same number of voxels a preprocess of all sequences have been done and in particular they were bring to a common reference system): (a,b) 2D slices at corresponding axial levels of the respective 3D images of the hearts at that moment. (c,d) slice of transformed image (b) after 3D registration on image (a) without (in (c)) and with (d) previous segmentation and masking of the endocardium. Note the misalignment of the approach without masking where a part of the right ventricle has been mapped onto the structure shown by the arrow in (a) and not belonging to the right ventricle. The regularization parameter was set to $\lambda_\rho = 5.0$ in both cases.

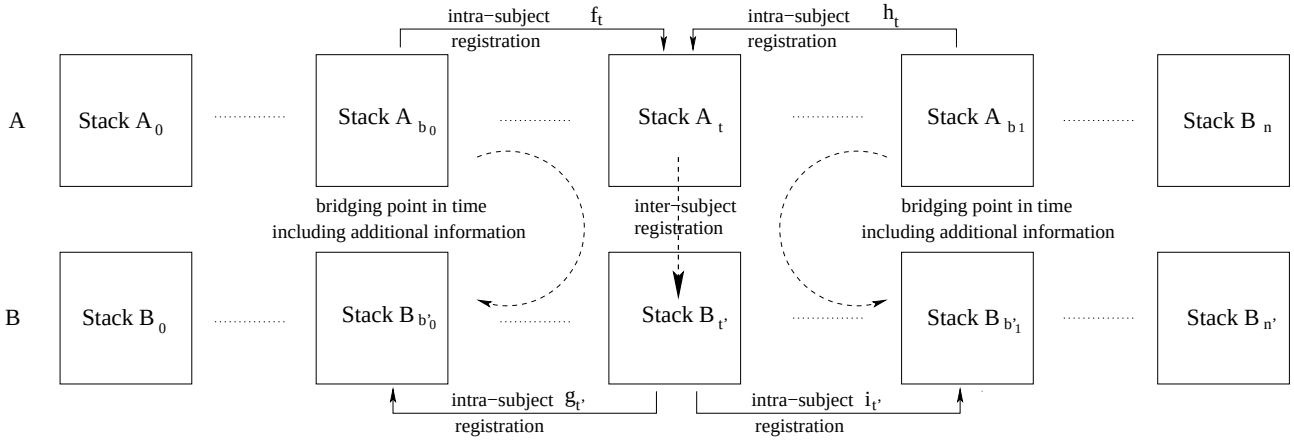

Figure 2. Overview of the bridging point registration approach. (t, t') is the current pair of points in time for which we want to obtain the 3D registration. The arrows point form the moving to the fixed images.

For that purpose, we segmented the first point in time of the cardiac cycle using the method introduced in (Fritscher and Schubert 2005) [7] based on statistical appearance models and level set segmentation (see also Section 4.1.).

3.2. Our approach: Bridging point registration

Here, we propose an approach, which we will call *bridging point registration*, for the registration of two 3D images A_i and $B_{i'}$ belonging to two 4D sequences (A and B) of different subjects, respectively. The approach allows to use additional information provided by the user for *one* single or *two* selected pair of points in time, namely by applying the masking based on a semiautomatic segmentation as described in Subsection 3.1.. Fig. 1(d) depicts the registration result using the masked image. The selected pairs of points in time we call bridging points (in time) A_{b_0}, A_{b_1} and $B_{b'_0}, B_{b'_1}$ (where A_i or $B_{i'}$, $i = b_0$ or $i = b_1$, $i' = b'_0$ or $i = b'_1$ belong to the sequences A or B, respectively). Here, we calculated first a temporal association between the images of the two sequences. We used a linear temporal alignment of the two sequences using temporal nearest neighbor interpolation.

If we consider a fixed point in time t and a given corresponding point in time $t' = T_{temp}(t)$ the calculation $T_{spat}(\cdot, t)$ might be achieved using purely spatial inter-subject registration. In our approach (see Fig. 2), we calculate first the *intra*-subject registration of A_{b_0} with respect to A_t, transforming image A_{b_0} (the *moving* image, c.f., Section 2.) on image A_t, obtaining the *intra-subject transformation* $f_t : \Omega_{A_t} \rightarrow \Omega_{A_{b_0}}$. Likewise, we perform the intra-subject registration transforming image $B_{t'}$ on image $B_{b'_0}$ obtaining the intra-subject transformation $g_{t'} : \Omega_{B_{b'_0}} \rightarrow \Omega_{B_{t'}}$. Correspondingly, we proceed with bridging point (b_1, b'_1) leading to the transformations h_t and $i_{t'}$ as depicted in Fig. 2.

These intra-subject transformations are used as input for the inter-subject registration of the two images A_t and $B_{t'}$ that we formulate as optimization problem with the following cost functional:

$$\begin{aligned} C(\mathbf{p}; \lambda_t, \lambda_{b_0}, \lambda_{b_1}) &= \lambda_t S(T_{spat}(\cdot, t; \mathbf{p}), A_t, B_{t'}) + \lambda_{b_0} S(f_t \circ T_{spat}(\cdot, t; \mathbf{p}) \circ g_{t'}, A_{b_0}, B_{b'_0}) \\ &\quad + \lambda_{b_1} S(h_t \circ T_{spat}(\cdot, t; \mathbf{p}) \circ i_{t'}, A_{b_1}, B_{b'_1}) + \lambda_\rho R(T_{spat}(\cdot, t; \mathbf{p})) \end{aligned} \quad (3)$$

where $T_{spat}(\cdot, t; \mathbf{p})$ denotes a parametric transformation with parameter vector $\mathbf{p}$ and within a transformation space $\mathcal{T}$, the weights λ_j are parameters to be fixed and $S(T, A_i, B_{i'})$ denotes the similarity measure quantifying how well image A_i transformed via T resembles to image $B_{i'}$. $R(T_{spat}(\cdot, t; \mathbf{p}))$ is a regularization term (see Section 2.). $f_t \circ T_{spat}(\cdot, t; \mathbf{p}) \circ g_{t'}$ denotes the concatenation of the transformations $g_{t'}, T_{spat}(\cdot, t; \mathbf{p}), f_t$ which leads to the successive transformation of image A_{b_0} in opposite direction (c.f., notations in Section 2.) as illustrated in Fig. 2. We used for intra- and inter-subject registration the normalized mutual information (NMI) similarity measure and successively a rigid, an affine and a multi-resolution B-spline based transformation as described in Section 2.We optimize $C(\mathbf{p}; \lambda_t, \lambda_{b_0}, \lambda_{b_1})$ with respect to $\mathbf{p}$ using the optimizer mentioned in Section 2.

In order to validate the quality of different direct (*standard*) registration approaches (using only the information of the images to be registered at the current pair of points in time of two 4D sequences) a protocol to assess the registration consistency within so-called *registration loops* has been developed and used in Pennec et al. [12] (see also Roche et al. [16]). A registration loop is given by the concatenation of the intra- and inter-subject transformations obtained by registration at two pairs of points in time and optimally it should lead to the identity. In contrast, our approach allows to use the transformation between images A_{b_0} and $B_{b'_0}$ as well as that between images A_{b_1} and $B_{b'_1}$ as an additional constraint for the registration of images A_t and $B_{t'}$ and hence, to transfer the information obtained by the registration for the bridging points to the other pairs of points in time (see Section 5. for further discussion). For evaluation (Section 4.2.), we register correspondingly image $B_{t'}$ on image A_t and take the direction minimizing the cost value for deciding if transforming image A_t on $B_{t'}$ or vice versa.

4. Evaluation and Results

4.1. Data and Evaluation Measures

We evaluated our approach using MR data from 8 healthy volunteers leading to 28 (undirected, and 56 directed) inter-subject combinations (see Table 1). The 8 image sequences have been acquired with a Siemens Sonata 1.5 T scanner and consist of cine breath-hold series of short axis slices. The original size of each pixel in each 3D image of each sequence was 1.56×1.56 mm and the slice thickness was 5 mm, the pixel number was 192×192 in each xy-plane and varied in z-direction with the size of the

heart. The length of the cardiac cycle varied from 500 to 720 msec and an image has been taken each 50 msec. (sequences of 10 up to 15 3D images). In order to create spatially isotropic data, the images have been resampled to a voxel size of $1.56 \times 1.56 \times 1.56$ mm using linear interpolation.

In order to evaluate our new approach we defined a distance measure based on the mean of point-wise distances of surface points. For that purpose (and not to use it for registration), we labeled the endocardial regions of different anatomical structures (Left Atrium, Left Ventricle, Right Atrium and Right Ventricle) and we extracted the corresponding endocardial surfaces also for all other points in time by using the segmentation result of the first point in time (see Section 3.2.) as an initial surface for semiautomatic segmentation [7] based on geodesic active contours (as implemented in the Insight Segmentation and Registration Toolkit (ITK) [22]). We applied the resulting transformation of the registration process to the surface of the corresponding subject among the two surfaces to compare. Given two set of surface points, let say S_1 and S_2, the mean distance $d(S_1, S_2)$ is the average of the distances between each point in both surfaces to the corresponding nearest point in the other surface, more precisely

$$d(S_1, S_2) = \frac{1}{n_1} \sum_{x \in S_1} \min_{y \in S_2} d(x, y) + \frac{1}{n_2} \sum_{y \in S_2} \min_{x \in S_1} d(x, y), \tag{4}$$

where $d(x, y)$ is the euclidean distance and n_i the cardinality of $S_i (i = 1, 2)$.

4.2. Registration Results

We assessed the quality of the registration using the evaluation measure introduced in Subsection 4.1.. Table 1 shows the mean distance results for the 2^{nd} and 4^{th} pairs of point in time after the first of the two selected bridging points (after the temporal alignment we selected frame 0 and frame 4 as bridging points), averaged over all 28 inter-subject combinations, before (identity) and after transforming surfaces (extracted for the purpose of validation only and not for registration) by the transformations obtained trough affine and B-spline bridging point registration. Using our B-spline multi-resolution scheme we added successively 2 control points to each grid line in each grid direction until a total resolution of $13 \times 13 \times 13$ control points is obtained. According to the observed quality measures values, the bridging point registration performs better in the right atrium and specially in the right ventricle compared to the direct 3D inter-subject registration using the same basic registration technique and the same parameter settings as for the bridging point registration. Moreover, for the direct registration we observe a less robust behavior and a high variability in the quality of results (up to mean distance values above $d = 5.0$). A notable improvement of the bridging-point registration results in the four structures under evaluation occurs when using not only the information at the bridging point but also at the point in time corresponding to the images to be registered ($\lambda_t = 0.5$, $\lambda_{b_0} = 0.5$, see the third and the fifth columns in Table 1). For each of these structures this improvement is valid between 20 (left ventricle, $time = 2$) and 28 (right atrium, $time = 4$) inter-subject registration processes from the 28 considered inter-subject comparisons. The improvement increases if we add a second bridging point b_1 in the registration process (evaluated for $t = 2$, only, as $b_1 = 4$). For the latter two settings of the weights we have, a better performance in all the structures compared to the direct registration and the setting ($\lambda_t = 0$, $\lambda_{b_0} = 1$). A strong improvement in the right ventricle (1.96 mm compares to 2.92 mm) and atrium (1.81 mm compares to 2.39 mm) was expected as the background structure making the registration process difficult as shown in Figure 1 appears only close to the right ventricle.

The computation time on a Pentium(R) D, 3.2GHz, amounts to 2h for the intra-subject registration from point in time 0 to point in time 4 (hence, for 4 different image pairs) and to 40 or 60 min for

		bridging-point registration						standard
		$time = t$, $\lambda_t = 0$ $b_0 = 0$, $\lambda_{b_0} = 1$		$time = t$, $\lambda_t = 0.5$ $b_0 = 0$, $\lambda_{b_0} = 0.5$		$time = t$, $\lambda_t = 0.33$ $b_0 = 0$, $\lambda_{b_0} = 0.33$ $b_1 = 4$, $\lambda_{b_1} = 0.33$		
	identity	affine	affine + bspline	affine	affine + bspline	affine	affine + bspline	affine + bspline
time $t = 2$								
Left Atrium	4.59	4.12	2.22	4.11	1.98	3.82	1.68	2.04
Left Ventricle	4.32	2.67	1.92	2.69	1.85	2.76	1.73	1.91
Right Atrium	5.17	4.07	2.24	4.10	2.06	3.80	1.79	2.39
Right Ventricle	5.19	2.88	2.21	3.05	2.12	2.96	1.95	2.92
time $t = 4$								
Left Atrium	4.67	4.13	2.36	4.10	2.09	—	—	2.24
Left Ventricle	4.26	2.66	2.07	2.62	1.89	—	—	1.79
Right Atrium	5.09	4.06	2.30	3.97	2.05	—	—	2.38
Right Ventricle	5.28	3.27	2.51	3.26	2.34	—	—	3.14

Table 1. Distance d in mm, mean over 28 inter-subject comparisons. The upper block of rows numbers correspond to the results of the inter-patient registration at frame time 2 whereas the lower one corresponds to point in time 4. The first column correspond to the values before registration. The next two pair of columns correspond to the results after bridging point registration based on affine and B-Spline transformations using $b_0 = 0$ as the only bridging point in time and respectively two different weight-settings for the terms in the cost functional (in this two cases, λ_{b_1}=0 in Eq. (3), it is omitted for sake of simplicity). In the next columns the result of including a second bridging point is shown for the case of registration at point in time 2 (see Eq. (3)). We did not test time frame 4 as $b_1 = 4$. Finally, the last column correspond to the direct gray level based registration (standard approach) results. Note that the mean distance improved up to 33% or 25%, respectively, using the bridging point registration compared to the standard approach in the right ventricle at time 2 or time 4, respectively.

inter-subject direct or bridging-point registration.

5. Discussion, Conclusion and Further Work

We proposed a method for the alignment of 3D images of corresponding points in time in two image sequences of different subjects using 4D information. The 4D information was brought in when calculating the spatial 3D registration for a given pair of points in time in both sequences by integrating constrains from the spatial inter-subject registration at other pairs of points in time concatenated with the intra-sequence motion relating the other points in time with the given pair of points in time. In particular, we use bridging points in time for which we allow interactive segmentation and we define a scheme making it possible to integrate the information obtained through the mentioned constrains into a single cost functional.

Our results based on 28 inter-subject combinations show that our bridging point approach outperforms a direct approach, in particular, in the right ventricle by 25% up to 33%. Interestingly, to integrate also gray-value information of the considered point in time (by setting $\lambda_t > 0$) improved notably the result even if no segmentation was performed in this point in time. Furthermore, the integration of a second bridging point in time led again to an additional appreciable improvement: from 6% (left ventricle) up to 16% (left atrium). Here, we used the first point in time and the point of maximum

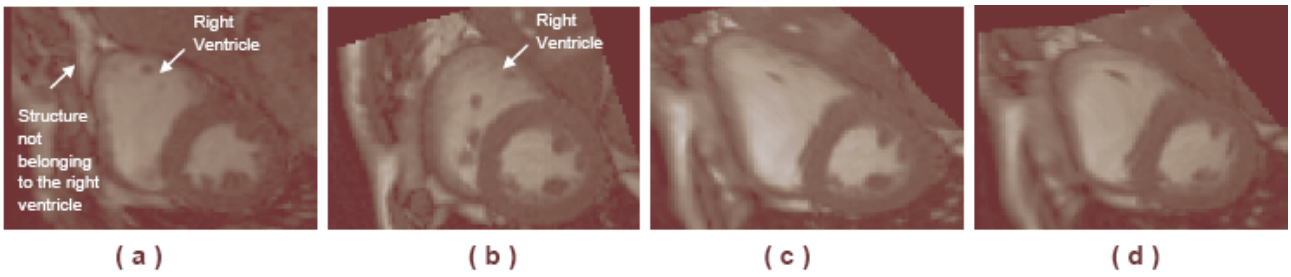

Figure 3. Illustration of the results obtained with our new approach compared to a direct normalized mutual information based inter-subject registration for the 4^{th} point in time of both image sequences, respectively. (a,b) 2D slices at corresponding axial levels of the respective 3D images of the heart at point in time 4. (c,d) slice of transformed image (b) after direct registration (c) and after our bridging-point approach ($t = 4$, $\lambda_t = 0.5$, $b_0 = 0$, $\lambda_{b_0} = 0.5$ in Eq. (3)) (d). With the direct approach again a part of the right ventricle has been mapped onto a structure that does not belong to the right ventricle (see arrow in (a)), leading to a strong mismatch. Our approach behaves robust and accurate in this situation.

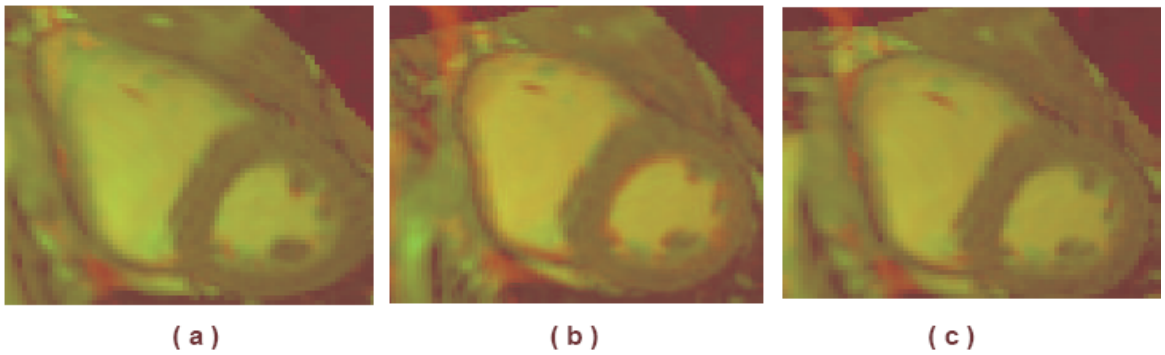

Figure 4. Overlaying of the 2D slices at the corresponding axial levels taken from the images at the 4^{th} point in time. The fixed image in red is superposed by the transformed moving image in green after direct (a) and bridging-point registration with associated cost functional defined in Eq. (3) with ($t = 4$, $\lambda_t = 0$, $b_0 = 0$, $\lambda_{b_0} = 1$) in (b) and with ($t = 4$, $\lambda_t = 0.5$, $b_0 = 0$, $\lambda_{b_0} = 0.5$) in (c). Note that in the latter case the resemblance in the left ventricle is better than in the former. Both bridging-point registration method (b,c) performs substantially better in the right ventricle compared to the standard approach (a).

contraction as bridging points in time. As a next step, we will test out other bridging points and the use of additional bridging points *not* coming with additional user information.

For the comparison of motion in different image sequences Rao et al. [15] calculated the motion fields with respect to the end-diastolic images, spatially registered the end-diastolic images, and transformed the motion fields based on the calculated transformation and on its inverse. Hence, *implicitly*, they make use of analogue spatial associations for the other points in time, compared to our approach with $\lambda_{b_0} = 1$, $\lambda_t = 0$ and $\lambda_{b_1} = 0$. The fact that we obtain better results using the settings $\lambda_{b_0} = 0.5$, $\lambda_t = 0.5$ and $\lambda_{b_1} = 0$ or $\lambda_{b_0} = 0.33$, $\lambda_t = 0.33$ and $\lambda_{b_1} = 0.33$ illustrates the limitation of an implicit use of the considered spatial associations compared to the *explicit* spatial registration for the other points in time in our approach. Similarly, trying to exploit the consistency property of registration loops by simply concatenating the transformations resulting from intra-subject registration and direct inter-subject registration in the bridging point would, additionally, *not* lead to a B-spline as the concatenation of two B-splines is not necessarily a B-spline.

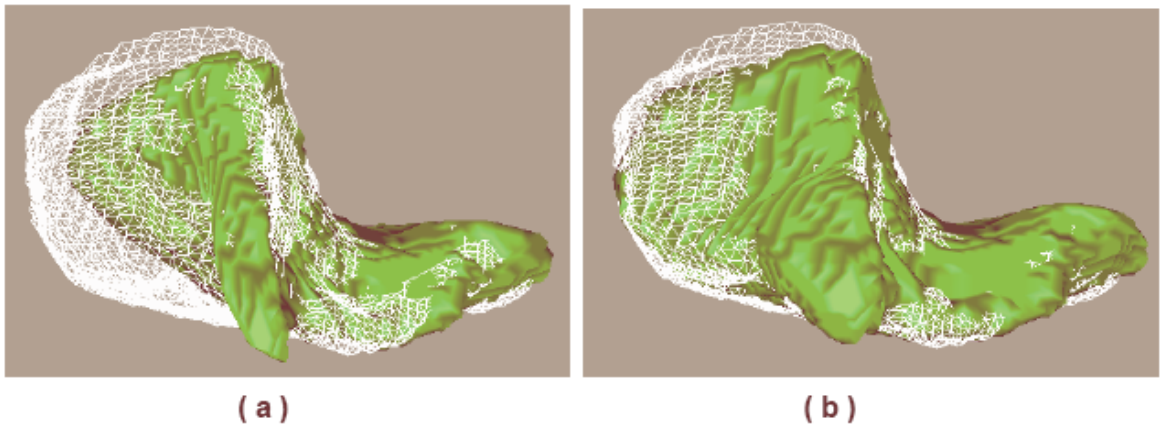

Figure 5. 3D wireframe rendering the endocardial surface of the right ventricle for the target subject and the overlaid 3D endocardial surface of the right ventricle for the transformed source subject. (a) Obtained after direct registration and (b) after our our bridging-point approach ($t = 4$, $\lambda_t = 0.5$, $b_0 = 0$, $\lambda_{b_0} = 0.5$ in Eq. (3)). The target subject is extracted from the image shown in Fig. 3(b) and the source subject from that shown in Fig. 3(a). Note that the surfaces have been extracted for the purpose of evaluation only; both registration methods do *not* use them.

Further applications of the 4D registration problem as formulated in Section 2. include the use of different reference points in time, for instance, for analyzing shape variation for different points in time or for compensating shape differences when transforming motion fields for far points in time. In Fig. 6 we present a first example for visualizing the differences in motion over the heart cycle of two different subject. The motion vectors belonging to one subject have been transformed to the other subject using the inverse of the Jacobian of the inter-subject transformation obtained by registration (c.f., Rao et al. [15]). Fig. 6 illustrates the additional information obtained by transforming the motion fields into the same reference system for *different* initial points in time. Currently, we investigate the use of an invertible inter-subject transformation in order to ensure that the inverse of the Jacobian exists in each point. Another application is the comparison of sequences acquired with different imaging modalities, e.g., SPECT and MRI.

For future work we plan to formulate our cost functional in terms of regions and to integrate an automatic decision about a local weighting of the terms corresponding to the different pairs of points in time. Additionally, we intend to apply our technique to investigate the evolution of the cardiac motion of patients suffering from myocarditis.

References

[1] U.E. Aladl, G.A. Hurwitz, D. Dey, D. Levin, M. Drangova, and P. Slomka. Automated registration of gated cardiac single-photon computed tomography and magnetic resonance imaging. *Journal of Magnetic Resonance Imaging*, 19:283–290, 2004.

[2] Y. Caspi and M. Irani. Spatio-temporal alignment of sequences. *IEEE Transactions on Pattern Analysis and Machine Intelligence*, 24:1409–1424, 2002.

[3] R. Chandrashekara, A. Rao, G. I. Sanchez-Ortiz, R. H. Mohiaddin, and D. Rueckert. Construction of a statistical model for cardiac motion analysis using non-rigid image registration. In

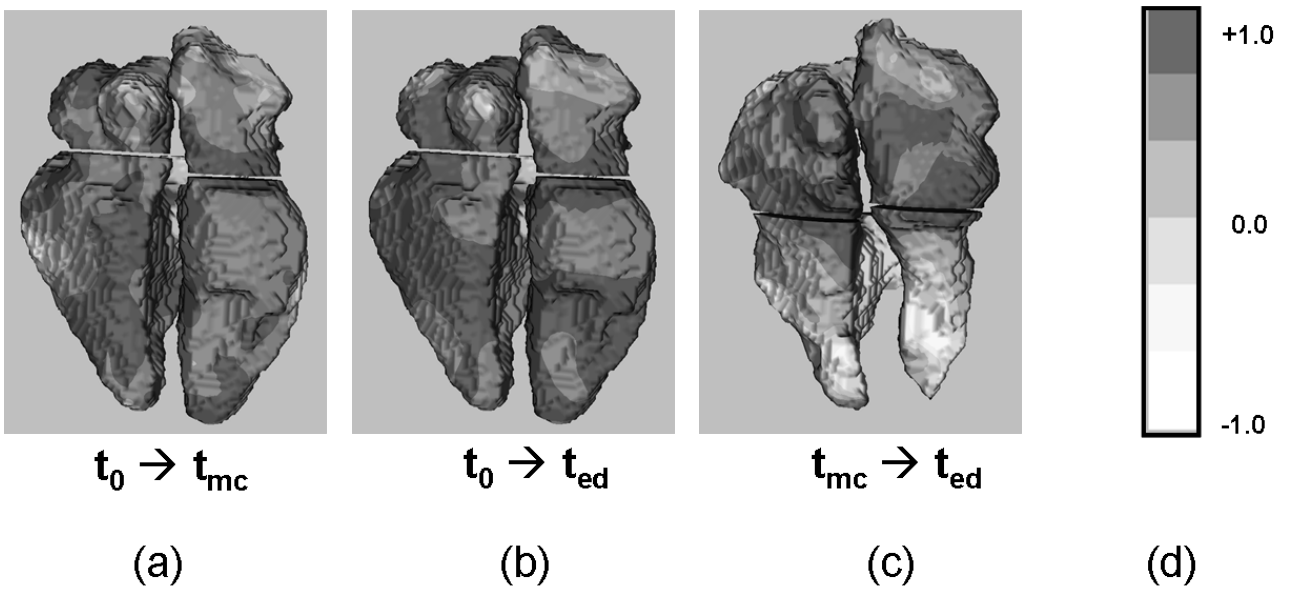

Figure 6. Visualization of the similarities and differences of the motion during the heart cycle of two different subjects. Based on the inter-subject transformation obtained by our registration approach the motion vectors have been transformed into the same reference system (see text) and the correlation between the motion vectors has been calculated pointwise and color coded (dark gray is high and light gray low correlation and white is high negative correlation, cf. (d)). (a) movements between the first point in time of the heart cycle and the point of maximum contraction are considered; (b) as in (a) but the second point in time is the end-diastole; (c) additional insight (e.g., negative correlation in the ventricles (below) in (c)) is obtained taking maximum contraction as first and end-diastole as second point in time.

Information Processing in Medical Imaging (IPMI '03), volume 2732 of *LNCS*, pages 599–610, 2003.

[4] T. F. Cootes, C. J. Taylor, D. H. Cooper, and J. Graham. Active shape models – their training and application. *Computer Vision and Image Understanding*, 61:38–59, 1995.

[5] Timothy F. Cootes, C. Beeston, Gareth J. Edwards, and Christopher J. Taylor. A unified framework for atlas matching using active appearance models. In *IPMI*, pages 322–333, 1999.

[6] T.L. Faber, R.W. McColl, R.M. Opperman, J.R. Corbett, and RM. Peshock. Spatial and temporal registration of cardiac SPECT and MR images: methods and evaluation. *Radiology*, 179:857–861, 1991.

[7] K. Fritscher and R. Schubert. A software framework for preprocessing and level-set segmentation of medical image data. In *SPIE Medical Imaging: Image Processing*, pages 1742–1752, 2005.

[8] R. Klabunde. *Cardiovascular Physiology Concepts*. Lippincott Williams and Wilkins, Washington, D.C., 2004.

[9] M. J. Ledesma-Carbayo, P. Mahia-Casado, A. Santos, E. Perez-David, M.A. Garcia-Fernandez, and M. Desco. Cardiac motion analysis from ultrasound sequences using nonrigid registration: validation against Doppler tissue velocity. *Ultrasound in Medicine and Biology*, 32(4):483–490, April 2006.

[10] A. Lopez, K.D. Fritscher, T. Trieb, R. Schubert, and J. Mattes. 3D Inter-Subject Cardiac Registration Using 4D Information. In *SPIE Medical Imaging 2008: Image Processing*, 2008 (in press).

[11] D. Mattes, D. R. Haynor, H. Vesselle, T. K. Lewellen, and W. Eubank. PET-CT Image registration in the chest using free-form deformations. *IEEE Transaction on Medical Imaging*, 22(1):120–128, January 2003.

[12] Xavier Pennec, Charles R. G. Guttmann, and Jean-Philippe Thirion. Feature-based registration of medical images: Estimation and validation of the pose accuracy. In *MICCAI '98: Proceedings of the First International Conference on Medical Image Computing and Computer-Assisted Intervention*, pages 1107–1114, London, UK, 1998. Springer-Verlag.

[13] D. Perperidis, M. Lorenzo-Valdes, R. Chandrashekara, A. Rao, R. Mohiaddin, G. I. Sanchez-Ortiz, and D. Rueckert. Building a 4D atlas of the cardiac anatomy and motion using MR imaging. In *IEEE ISBI'04*, pages 412–415, 2004.

[14] D. Perperidis, R. H. Mohiaddin, and D. Rueckert. Spatio-temporal free-form registration of cardiac MR image sequences. *Medical Image Analysis*, 9:441–456, 2005.

[15] A. Rao, R. Chandrashekara, G.I. Sanchez-Ortiz, R. Mohiaddin, P. Aljabar, J.V. Hajnal, B.K. Puri, and D. Rueckert. Spatial transformation of motion and deformation fields using nonrigid registration. *IEEE Transaction on Medical Imaging*, 23:1065–1076, 2004.

[16] Alexis Roche, Xavier Pennec, Grégoire Malandain, and Nicholas Ayache. Rigid Registration of 3D Ultrasound with MR Images: A New Approach Combining Intensity and Gradient Information. *IEEE Trans. Med. Imaging*, 20(10):1038–1049, 2001.

[17] N. Rougon, C. Petitjean, and F. Prêteux. Building and using a statistical 3D motion atlas for analyzing myocardial contraction in MRI. In *SPIE Medical Imaging'04: Image Processing, San Diego, CA*, volume 5370, pages 253–264, 14-19 February 2004.

[18] T. W. Sederberg and S. R. Parry. Free-form deformations of solid geometric models. *Computer Graphics (SIGGRAPH'86)*, 20(4):151–160, 1986.

[19] C. Studholm, D. L. G. Hill, and D. J. Hawkes. An overlap invariant entropy measure of 3D medical image alignment. *Pattern Recognition*, 32:71–86, 1999.

[20] R. Szeliski. *Bayesian Modeling of Uncertainty in Low-Level Vision*. Kluwer Academic Publisher, Boston, Massachusetts, 1989.

[21] T. G. Turkington, T. R. DeGrado, M. W. Hanson, and R. E. Coleman. Alignment of dynamic cardiac PET images for correction of motion. *IEEE Trans. Nucl. Sci.*, 44:235–242, 1997.

[22] T. S. Yoo, editor. *Insight into Images: Principles and Practices for Segmentation, Registration and Image Analysis*. published by A.K. Peters, 2004.

[23] Weiwei Zhang, J. Alison Noble, and J. Michael Brady. Spatio-temporal Registration of Real Time 3D Ultrasound to Cardiovascular MR Sequences. In *MICCAI (1)*, pages 343–350, 2007.

(S, N)- and R-implications: a state-of-the-art survey

Balasubramaniam Jayaram
Dept. of Mathematics, Faculty of Civil Engineering
Slovak University of Technology, 81368 Bratislava, Slovakia

Abstract

In this work we give a state-of-the-art review of two of the most established classes of fuzzy implication operations, viz., (S, N)- and R-implications. Firstly, we discuss their properties, characterizations and representations. Using the presented facts, an almost complete characterization of the intersections that exist among some subfamilies of (S, N)- and R-implications are obtained.

Keywords: fuzzy implication, functional equations, uninorm.

1 Introduction

Fuzzy implications were introduced and studied in the literature as the generalization of the classical implication operation. Following are the two main ways of defining an implication in the Boolean lattice $(L, \wedge, \vee, \neg)$:

$$p \to q \equiv \neg p \vee q, \tag{1}$$
$$p \to q \equiv \max\{t \in L \mid p \wedge t \leq q\}, \tag{2}$$

where $p, q \in L$ and the relation $\leq$ is defined in the usual way, i.e., $p \leq q$ iff $p \vee q = q$, for every $p, q \in L$. The implication (1) is usually called the material implication, while (2) is from the intuitionistic logic framework, where the implication is obtained as the residuum of the conjunction, and is often called as the pseudocomplement of p relative to q. Interestingly, despite their different formulas, definitions (1) and (2) are equivalent in the Boolean lattice $(L, \wedge, \vee, \neg)$. On the other hand, in the fuzzy logic framework, where the truth values can vary in the unit interval $[0, 1]$, the natural generalizations of the above definitions, viz., (S, N)- and R-implications, are not equivalent. This diversity is more a boon than a bane and has led to some intensive research on fuzzy implications for close to three decades. Quite understandably then, the most established and well-studied classes of fuzzy implications are the above (S, N)- and R-implications.

The main goal of this article is to give a state-of-the-art survey of these two families of fuzzy implications by discussing their algebraic properties, characterizations, representations and presenting both existing and some new results connected with their intersections.

2 Preliminaries: basic fuzzy logic connectives

We assume that the reader is familiar with the classical results concerning basic fuzzy logic connectives, and all the notations used in the text must be contextually clear. Only some definitions that are important in the sequel are given.

A generalization of the law of excluded middle, which in the classical case has the following form $p \vee \neg p = \top$, is as follows:

Definition 1. *Let S be a t-conorm and N a fuzzy negation. We say that the pair (S, N) satisfies the law of excluded middle if*

$$S(N(x), x) = 1, \qquad x \in [0, 1]. \tag{LEM}$$

One can associate a fuzzy negation to any t-norm or t-conorm as given in the definition below.

Definition 2. *Let T be a t-norm and S a t-conorm. The functions N_T, N_S defined as*

$$N_T(x) = \sup\{t \in [0,1] \mid T(x,t) = 0\},$$
$$N_S(x) = \inf\{t \in [0,1] \mid S(x,t) = 1\},$$

are called the natural negations of T and S, resp., where $x \in [0,1]$.

Remark 1. *(i) Notice that if $S(x,y) = 1$ for some $x, y \in [0,1]$, then $y \geq N_S(x)$ and if $T(x,y) = 0$ for some $x, y \in [0,1]$, then $y \leq N_T(x)$.*

(ii) If the pair (S,N) satisfies (LEM) *then $N \geq N_S$.*

Example 1. *Table 1 gives the natural negations of the basic t-norms and t-conorms, where*

$$N_{\mathbf{D1}}(x) = \begin{cases} 1, & \text{if } x = 0, \\ 0, & \text{if } x > 0, \end{cases}$$
$$N_{\mathbf{D2}}(x) = \begin{cases} 1, & \text{if } x < 1, \\ 0, & \text{if } x = 1. \end{cases}$$
$$N_{\mathbf{C}}(x) = 1 - x\ .$$

Table 1: Examples of natural negations

t-norm T	N_T	t-conorm S	N_S
positive	$N_{\mathbf{D1}}$	positive	$N_{\mathbf{D2}}$
$T_{\mathbf{LK}}$	$N_{\mathbf{C}}$	$S_{\mathbf{LK}}$	$N_{\mathbf{C}}$
$T_{\mathbf{D}}$	$N_{\mathbf{D2}}$	$S_{\mathbf{D}}$	$N_{\mathbf{D1}}$
$T_{\mathbf{nM}}$	$N_{\mathbf{C}}$	$S_{\mathbf{nM}}$	$N_{\mathbf{C}}$

The following relation exists between N_T and N_S of a De Morgan triple.

Theorem 1. *Let T be a left-continuous t-norm and S be a t-conorm. If (T, N_T, S) is a De Morgan triple, then*

(i) $N_S = N_T$ is a strong negation,

(ii) S is right-continuous.

3 Fuzzy implications and basic algebraic properties

In the literature, especially at the beginnings, we can find several different definitions of fuzzy implications. We will use the following definition (see [5]).

Definition 3. *A function $I\colon [0,1]^2 \to [0,1]$ is called a fuzzy implication if, for all $x, y, z \in [0,1]$, it satisfies*

$$I(x,z) \geq I(y,z) \quad \text{if} \quad x \leq y, \tag{I1}$$
$$I(x,y) \geq I(x,z) \quad \text{if} \quad y \geq z, \tag{I2}$$
$$I(0,0) = 1, \quad I(1,1) = 1, \quad I(1,0) = 0. \tag{I3}$$

Table 2: Examples of basic fuzzy implications

Name	Formula
Łukasiewicz	$I_{\mathbf{LK}} : \min(1, 1-x+y)$
Gödel	$I_{\mathbf{GD}} : \begin{cases} 1, & \text{if } x \leq y \\ y, & \text{if } x > y \end{cases}$
Reichenbach	$I_{\mathbf{RC}} : 1 - x + xy$
Kleene-Dienes	$I_{\mathbf{KD}} : \max(1-x, y)$
Goguen	$I_{\mathbf{GG}} : \begin{cases} 1, & \text{if } x \leq y \\ \frac{y}{x}, & \text{if } x > y \end{cases}$
Rescher	$I_{\mathbf{RS}} : \begin{cases} 1, & \text{if } x \leq y \\ 0, & \text{if } x > y \end{cases}$
Yager	$I_{\mathbf{YG}} : \begin{cases} 1, & \text{if } x = 0 \text{ and } y = 0 \\ y^x, & \text{if } x > 0 \text{ or } y > 0 \end{cases}$
Weber	$I_{\mathbf{TD}} : \begin{cases} 1, & \text{if } x < 1 \\ y, & \text{if } x = 1 \end{cases}$
Fodor	$I_{\mathbf{FD}} : \begin{cases} 1, & \text{if } x \leq y \\ \max(1-x, y), & \text{if } x > y \end{cases}$

Definition 4. *Let $x, y, z \in [0,1]$. A fuzzy implication I is said to satisfy*

(i) the left neutrality property, if

$$I(1,y) = y, \tag{NP}$$

(ii) the exchange principle, if

$$I(x, I(y,z)) = I(y, I(x,z)), \tag{EP}$$

(iii) the identity principle, if

$$I(x,x) = 1, \tag{IP}$$

(iv) the ordering property, if

$$x \leq y \iff I(x,y) = 1, \qquad \text{(OP)}$$

(v) the law of contraposition with respect to a fuzzy negation N, CP(N), if

$$I(x,y) = I(N(y), N(x)). \qquad \text{(CP)}$$

Just as in the case of t-norms or t-conorms, a fuzzy negation can be obtained from fuzzy implications too as follows.

Definition 5. *If I is a fuzzy implication, then the function $N_I\colon [0,1] \to [0,1]$ defined by*

$$N_I(x) = I(x,0), \qquad x \in [0,1],$$

is called the natural negation of I.

4 (S,N)-implications: properties and characterizations

It is well-known in the classical logic that the unary negation operation $\neg$ can combine with any other binary operation to generate rest of the binary operations. This distinction of the unary $\neg$ is also shared by the Boolean implication $\to$, if defined in the following usual way:

$$p \to q \equiv \neg p \vee q.$$

The definition as given above was the first to catch the attention of the researchers leading to the following class of fuzzy implications.

4.1 Definition and examples

Definition 6 (cf. [5])**.** *A function $I\colon [0,1]^2 \to [0,1]$ is called an (S,N)-implication if there exists a t-conorm S and a fuzzy negation N such that*

$$I(x,y) = S(N(x), y), \qquad x,y \in [0,1]. \quad (3)$$

If N is a strong negation, then I is called a strong implication (shortly S-implication). We will denote it by $I_{S,N}$.

Example 2. *The following Table 3 lists few of the well-known (S,N)-implications along with the underlying t-conorms and fuzzy negations.*

Table 3: Examples of basic (S,N)-implications

S	N	(S,N)-implication $I_{S,N}$
$S_{\mathbf{M}}$	$N_{\mathbf{C}}$	$I_{\mathbf{KD}}$
$S_{\mathbf{P}}$	$N_{\mathbf{C}}$	$I_{\mathbf{RC}}$
$S_{\mathbf{LK}}$	$N_{\mathbf{C}}$	$I_{\mathbf{LK}}$
$S_{\mathbf{D}}$	$N_{\mathbf{C}}$	$I_{\mathbf{DC}}: \begin{cases} y, & \text{if } x = 1 \\ 1-x, & \text{if } y = 0 \\ 1, & \text{otherwise} \end{cases}$
$S_{\mathbf{nM}}$	$N_{\mathbf{C}}$	$I_{\mathbf{FD}}$
any S	$N_{\mathbf{D1}}$	$I_{\mathbf{D}}: \begin{cases} 1, & \text{if } x = 0 \\ y, & \text{if } x > 0 \end{cases}$
any S	$N_{\mathbf{D2}}$	$I_{\mathbf{TD}}$
$S_{\mathbf{M}}$	$1-x^2$	$I_{\mathbf{MK}}: \max(1-x^2, y)$

4.2 Properties of (S,N)-implications

In this section we analyze (S,N)-implications with respect to the algebraic properties given in Definition 4. We begin with the following remark.

Remark 2 (see [9, 2])**.** *(i) All (S,N)-implications are fuzzy implications which satisfy* (NP) *and* (EP)*.*

(ii) If I is an (S,N)-implication obtained from a fuzzy negation N, then $N = N_I$.

(iii) An $I_{S,N}$ satisfies CP(N) with some fuzzy negation N if and only if $N = N_I$ is a strong negation, i.e., $I_{S,N}$ is an S-implication.

Since not all (S,N)-implications satisfy the identity principle (IP) and, hence, the ordering property (OP) (for example $I_{\mathbf{RC}}$ and $I_{\mathbf{KD}}$), we analyze these axioms for (S,N)-implications now.

Lemma 1. *For a t-conorm S and a fuzzy negation N, the following are equivalent:*

(i) An $I_{S,N}$ satisfies (IP)*.*

(ii) The pair (S,N) satisfies (LEM)*.*

Theorem 2. *For a t-conorm S and a fuzzy negation N, the following are equivalent:*

(i) An $I_{S,N}$ satisfies (OP)*.*

(ii) $N = N_S$ is a strong negation and the pair (S, N_S) satisfies (LEM)*.*

4.3 Characterizations and representations of (S,N)-implications

A first characterization of S-implications was presented by Trillas and Valverde [9] (see also [5]) and it can be written in the following form.

Theorem 3. *For a function* $I\colon [0,1]^2 \to [0,1]$ *the following are equivalent:*

(i) I *is an* S*-implication.*

(ii) I *satisfies* (I1) *(or* (I2)*),* (NP)*,* (EP) *and* (CP) *with respect to a strong negation* N*.*

The characterization of the family of all (S,N)-implications is still an open problem, but some partial results were recently obtained in [2].

Theorem 4 ([2], Theorems 2.6, 5.1 and 5.2)**.** *For a function* $I\colon [0,1]^2 \to [0,1]$ *the following statements are equivalent:*

(i) I *is an* (S,N)*-implication generated from some t-conorm* S *and some continuous (strict, strong) fuzzy negation* N*.*

(ii) I *satisfies* (I1) *(or* (I2)*),* (EP) *and the function* N_I *is a continuous (strict, strong) fuzzy negation.*

Moreover, the representation of the (S,N)*-implication* (3) *is unique in this case.*

It should be noted that the properties in Theorem 4 are mutually independent (see [2]).

In the class of continuous function we have the following important result.

Proposition 1. *For a function* $I\colon [0,1]^2 \to [0,1]$ *the following are equivalent:*

(i) I *is a continuous* (S,N)*-implication.*

(ii) I *is an* (S,N)*-implication with continuous* S *and* N*.*

Finally, we are able to prove one of the most important results connected with (S,N)-implications. It is usually called in the literature as Smets-Magrez Theorem, since the equivalence between points (i) and (v) was presented in [8]. We would like to note, that a similar result was obtained by Trillas and Valverde two years earlier (see [9], Theorem 3.4). In fact, in the article [8], the authors required more conditions than it is necessary (see [5], Theorem 1.15).

Theorem 5 (cf. [9, 8, 5])**.** *For a function* $I\colon [0,1]^2 \to [0,1]$ *the following statements are equivalent:*

(i) I *is continuous and satisfies* (EP)*,* (OP)*.*

(ii) I *is an* (S,N)*-implication obtained from a continuous t-conorm* S *and a continuous negation* N*, which satisfies* (OP)*.*

(iii) I *is a continuous* (S,N)*-implication, which satisfies* (OP)*.*

(iv) I *an* (S,N)*-implication obtained from a nilpotent t-conorm and its natural negation.*

(v) I *is isomorphic to the Łukasiewicz implication* $I_{\mathbf{LK}}$*.*

Remark 3. *The continuity of the t-conorm* S *is important in the above theorem. Consider the Fodor implication* $I_{\mathbf{FD}}$*. It is a non-continuous* (S,N)*-implication, not isomorphic to the Łukasiewicz implication and obtained from the right continuous t-conorm* $S_{\mathbf{nM}}$*. But it satisfies both* (EP) *and* (OP)*.*

5 R-implications: properties and characterizations

From the isomorphism that exists between classical two-valued logic and classical set theory one can immediately note the following set theoretic identity:

$$\overline{P} \cup Q = \overline{P \setminus Q} = \cup \{T \mid P \cap T \subseteq Q\}\,,$$

where P, Q are subsets of some universal set. The above identity gives another way of defining the Boolean implication and is employed in the intuitionistic logic. Fuzzy implications obtained as the generalization of the above identity form the family of residuated implications, usually called as R-implications in

the literature. In this section, we investigate properties they possess, analogous to our treatment of (S, N)-implications in Section 4.

5.1 Definition and examples

Definition 7 (see [5]). *A function $I\colon [0,1]^2 \to [0,1]$ is called an R-implication if there exists a t-norm T such that, for all $x, y \in [0,1]$,*

$$I(x,y) = \sup\{t \in [0,1] \mid T(x,t) \leq y\}. \quad (4)$$

If an R-implication is generated from a t-norm T, then we will often denote this by I_T.

Firstly, observe that since for any t-norm T and all $x \in [0,1]$ we have $T(x,0) = 0$, the appropriate set in (4) is non-empty. It is very important to note that the name 'R-implication' is a short version of 'residual implication', and I_T is also called as 'the residuum of T'. This class of implications is related to a residuation concept from the intuitionistic logic. In fact, in this context this name is proper only for left-continuous t-norms.

Proposition 2 (cf. [6]). *For a t-norm T the following are equivalent:*

(i) T is left-continuous.

(ii) T and I_T form an adjoint pair, i.e., for any $x, y, t \in [0,1]$, they satisfy the residuation property

$$T(x,t) \leq y \iff I_T(x,y) \geq t. \quad \text{(RP)}$$

(iii) The supremum in (4) is the maximum.

Example 3. *Table 4 lists few of the well-known R-implications along with their t-norms from which they have been obtained. Note that $T_{\mathbf{D}}$ is not left-continuous but still $I_{\mathbf{TD}}$ is a fuzzy implication.*

5.2 Properties of R-implications

Now we examine R-implications based on the properties introduced in Section 3.

Theorem 6 (cf. [5]). *If T is any t-norm (not necessarily left-continuous), then $I_T \in \mathcal{FI}$. Moreover, I_T satisfies* (NP) *and* (IP).

Table 4: Examples of basic R-implications

t-norm T	R-implication I_T
$T_{\mathbf{M}}$	$I_{\mathbf{GD}}$
$T_{\mathbf{P}}$	$I_{\mathbf{GG}}$
$T_{\mathbf{LK}}$	$I_{\mathbf{LK}}$
$T_{\mathbf{D}}$	$I_{\mathbf{TD}}$
$T_{\mathbf{nM}}$	$I_{\mathbf{FD}}$

Without additional assumptions on a t-norm T, the residual implication I_T may not satisfy other basic properties. Such examples will be presented in the talk. On the other hand, we have:

Theorem 7 (see [5], Theorem 1.14). *If I_T is an R-implication based on a left-continuous t-norm T, then $I_T \in \mathcal{FI}$ and I_T satisfies* (NP), (EP), (IP), (OP). *Moreover, I_T is left-continuous with respect to the first variable and right-continuous with respect to the second variable.*

5.3 Characterizations and representations of R-implications

Our main goal in this subsection is to present the characterization of R-implications. In fact, presently such a characterization is available only for R-implications obtained from left-continuous t-norms. We also discuss the representations of R-implications for some special classes of left-continuous t-norms. To do this we consider the dual situation now, i.e., a method of obtaining t-norms from fuzzy implications. Since for every fuzzy implication I we have $I(x,1) = 1$, for all $x \in [0,1]$, the following function $T_I\colon [0,1]^2 \to [0,1]$ defined by, for all $x, y \in [0,1]$,

$$T_I(x,y) = \inf\{t \in [0,1] \mid I(x,t) \geq y\}, \quad (5)$$

is a well defined function of two variables and similar to Proposition 2 we have:

Proposition 3. *For a fuzzy implication I the following are equivalent:*

(i) I is right-continuous with respect to the second variable.

(ii) I and T_I form an adjoint pair, i.e., they satisfy (RP).

(iii) The infimum in (5) *is the minimum.*

Remark 4. *It is interesting to note, that formula* (5) *does not always generate a t-norm. For example, if I is the Reichenbach implication $I_{\mathbf{RC}}$, then for $x > 0$ we obtain $T_{I_{\mathbf{RC}}}(x, 1) = 1$, so $T_{I_{\mathbf{RC}}}$ is not a t-norm.*

Using similar techniques as in the proof of Theorem 7 one can prove the following result.

Theorem 8. *If $I \in \mathcal{FI}$ satisfies* (EP), (OP) *and is right-continuous with respect to the second variable, then T_I defined by* (5) *is a left-continuous t-norm. Moreover $I = I_{T_I}$.*

From Theorems 7 and 8 we get the following well-known characterization of R-implications generated from left-continuous t-norms.

Corollary 1 (cf. [7])**.** *For a function $I\colon [0,1]^2 \to [0,1]$ the following are equivalent:*

(i) I is an R-implication generated from a left-continuous t-norm.

(ii) I satisfies (I2), (EP), (OP) *and is right continuous with respect to the second variable.*

It should be noted, that in contrast to the characterization of (S,N)-implications the problem of mutual-independence of the above properties is still an open problem.

For continuous R-implications we have the following result, which is an other version of Theorem 5.

Theorem 9. *For a function $I\colon [0,1]^2 \to [0,1]$ the following are equivalent:*

(i) I is continuous and satisfies (EP), (OP)*.*

(ii) I is a continuous R-implication based on some left-continuous t-norm.

(iii) I is an R-implication based on some continuous t-norm, with a strong natural negation N_I.

(iv) I is an R-implication based on some nilpotent t-norm.

(v) I is isomorphic to the Łukasiewicz implication $I_{\mathbf{LK}}$.

6 Intersections among families of (S,N)- and R-implications

In this section, we discuss the different overlaps that exist between the above families. Let us denote the different families of fuzzy implications as follows:

- $\mathbb{I}_{\mathbb{S},\mathbb{N}}$ – the family of all (S,N)-implications;
- ${}^{\mathbb{C}}\mathbb{I}_{\mathbb{S},\mathbb{N}}$ – the family of all continuous (S,N)-implications;
- $\mathbb{I}_{\mathbb{S}_{\mathbb{C}},\mathbb{N}_{\mathbb{C}}}$ – the family of all (S,N)-implications obtained from continuous t-conorms and continuous negations;
- $\mathbb{I}_{\mathbb{S}}$ – the family of all S-implications;
- $\mathbb{I}_{\mathbb{S},\mathbb{N}_{\mathbb{S}}}$ – the family of all (S,N)-implications obtained from t-conorms and their natural negations;
- $\mathbb{I}_{\mathbb{S}^*,\mathbb{N}_{\mathbb{S}}^*}$ – the family of all (S,N)-implications obtained from right-continuous t-conorms and their natural negations which are strong;
- $\mathbb{I}_{\mathbb{T}}$ – the family of all R-implications;
- ${}^{\mathbb{C}}\mathbb{I}_{\mathbb{T}}$ – the family of all continuous R-implications;
- $\mathbb{I}_{\mathbb{T}_{\mathbb{LC}}}$ – the family of all R-implications obtained from left-continuous t-norms;
- ${}^{\mathbb{C}}\mathbb{I}_{\mathbb{T}_{\mathbb{LC}}}$ – the family of all continuous R-implications obtained from left-continuous t-norms;
- $\mathbb{I}_{\mathbb{T}_{\mathbb{C}}}$ – the family of all R-implications obtained from continuous t-norms;
- ${}^{\mathbb{C}}\mathbb{I}_{\mathbb{T}_{\mathbb{C}}}$ – the family of all continuous R-implications obtained from continuous t-norms;
- $\mathbb{I}_{\mathbb{LK}}$ – the family of all implications isomorphic to the Łukasiewicz implication $I_{\mathbf{LK}}$.

In the following two subsections, we summarize the known intersections between

the above subfamilies of (S,N)- and R-implications based on the results cited and obtained earlier, which is also diagrammatically represented in Figures 1 and 2. Following this, we discuss the relationships between families of (S,N)- and R-implications. The final result will also be diagrammatically represented.

6.1 Intersections between subfamilies of (S,N)-implications

From Proposition 1, we get

$$^{\mathbb{C}}\mathbb{I}_{\mathbb{S},\mathbb{N}} = \mathbb{I}_{\mathbb{S}_{\mathbb{C}},\mathbb{N}_{\mathbb{C}}}.$$

From Tables 1 and 3, Remark 2 (ii) and since isomorphism preserves (NP), (EP) and (OP), we have that

$$\begin{aligned}\mathbb{I}_{\mathbb{LK}} &= \mathbb{I}_{\mathbb{S},\mathbb{N}_{\mathbb{S}}} \cap \mathbb{I}_{\mathbb{S}_{\mathbb{C}},\mathbb{N}_{\mathbb{C}}} \\ &= \mathbb{I}_{\mathbb{S}_{\mathbb{C}},\mathbb{N}_{\mathbb{C}}} \cap \mathbb{I}_{\mathbb{S}^*,\mathbb{N}_{\mathbb{S}}^*} \\ &\subsetneq \mathbb{I}_{\mathbb{S}^*,\mathbb{N}_{\mathbb{S}}^*} \subsetneq \mathbb{I}_{\mathbb{S},\mathbb{N}_{\mathbb{S}}} \cap \mathbb{I}_{\mathbb{S}}.\end{aligned}$$

6.2 Intersections between subfamilies of R-implications

By Theorem 9, we have

$$^{\mathbb{C}}\mathbb{I}_{\mathbb{T}_{\mathbb{LC}}} = \mathbb{I}_{\mathbb{LK}}.$$

Quite obviously, we have the following containments:

$$^{\mathbb{C}}\mathbb{I}_{\mathbb{T}_{\mathbb{LC}}} = \mathbb{I}_{\mathbb{LK}} \subsetneq \mathbb{I}_{\mathbb{T}_{\mathbb{C}}} \subsetneq \mathbb{I}_{\mathbb{T}_{\mathbb{LC}}} \subsetneq \mathbb{I}_{\mathbb{T}}.$$

Similarly we get

$$^{\mathbb{C}}\mathbb{I}_{\mathbb{T}} \cap \mathbb{I}_{\mathbb{T}_{\mathbb{C}}} = {}^{\mathbb{C}}\mathbb{I}_{\mathbb{T}} \cap \mathbb{I}_{\mathbb{T}_{\mathbb{LC}}} = {}^{\mathbb{C}}\mathbb{I}_{\mathbb{T}_{\mathbb{C}}} = {}^{\mathbb{C}}\mathbb{I}_{\mathbb{T}_{\mathbb{LC}}} = \mathbb{I}_{\mathbb{LK}}.$$

It is still an open problem to find, if there exists, a continuous R-implication generated from a non-continuous t-norm.

6.3 Intersections between families of (S,N)- and R-implications

One of the first works on the intersection of S- and R-implications was done by Dubois and Prade [4], wherein they have shown that S-implications and R-implications could be merged into a single family, provided that the class of triangular norms is enlarged to non-commutative conjunction operations.

Firstly, note that since $I_{\mathbf{TD}}$ is both an (S,N)- and R-implication, we have

$$I_{\mathbf{TD}} \in \mathbb{I}_{\mathbb{S},\mathbb{N}} \cap \mathbb{I}_{\mathbb{T}} \neq \emptyset,$$

i.e., the intersection of (S,N)- and R-implications is non-empty. From Theorems 3, 7 and 9, we get

$$\mathbb{I}_{\mathbb{S}} \cap \mathbb{I}_{\mathbb{T}_{\mathbb{C}}} = \mathbb{I}_{\mathbb{LK}}.$$

On the other hand, by Theorem 5 and Corollary 1, we have

$$^{\mathbb{C}}\mathbb{I}_{\mathbb{S},\mathbb{N}} \cap \mathbb{I}_{\mathbb{T}_{\mathbb{LC}}} = \mathbb{I}_{\mathbb{LK}}.$$

The weaker version of the above two results is well known in the scientific literature and, in general, we say that the only continuous S-implication and R-implication (generated from a left-continuous t-norm) is the Łukasiewicz implication (up to an isomorphism). However, there are many R-implications obtained from t-norms that are left-continuous but non-continuous and are still S-implications, for example the Fodor implication $I_{\mathbf{FD}}$.

Let us denote by

- $\mathbb{I}_{\mathbb{T}^*}$ – the family of all R-implications obtained from left-continuous t-norms having strong induced negations.

It is clear now from our discussion, that

$$\mathbb{I}_{\mathbb{S}} \cap \mathbb{I}_{\mathbb{T}_{\mathbb{LC}}} = \mathbb{I}_{\mathbb{T}^*} \supsetneq \mathbb{I}_{\mathbb{LK}}.$$

Many families of left-continuous t-norms (up to a conjugation) with strong induced negations are known in the literature (see the works of Jenie, Maes and De Baets).

A characterization of the fuzzy implications that fall under the following intersections has been given recently in [3]:

$$\mathbb{I}_{\mathbb{S}} \cap \mathbb{I}_{\mathbb{T}_{\mathbb{LC}}} = \mathbb{I}_{\mathbb{S},\mathbb{N}} \cap \mathbb{I}_{\mathbb{T}_{\mathbb{LC}}} = \mathbb{I}_{\mathbb{N}_{\mathbb{T}}(\mathbb{T}),\mathbb{N}_{\mathbb{T}}} = \mathbb{I}_{\mathbb{T}^*},$$

where

Figure 1: Intersections among the subfamilies of (S, N)-implications

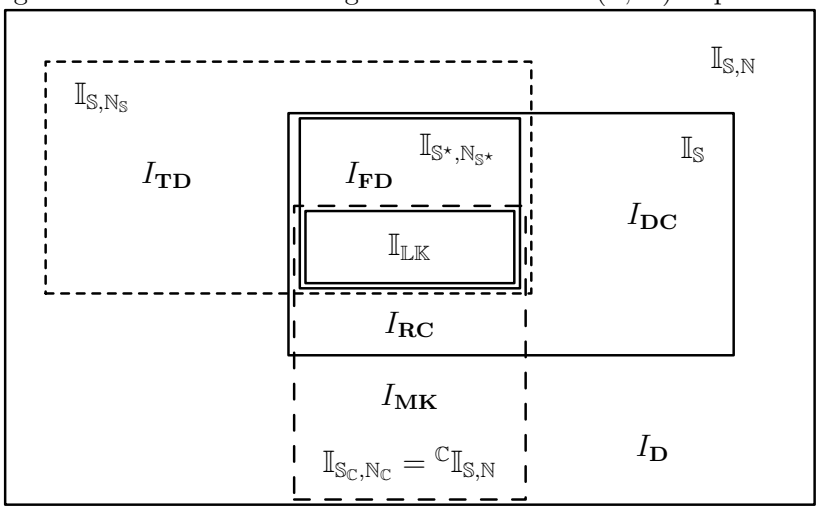

Figure 2: Intersections among the subfamilies of R-implications

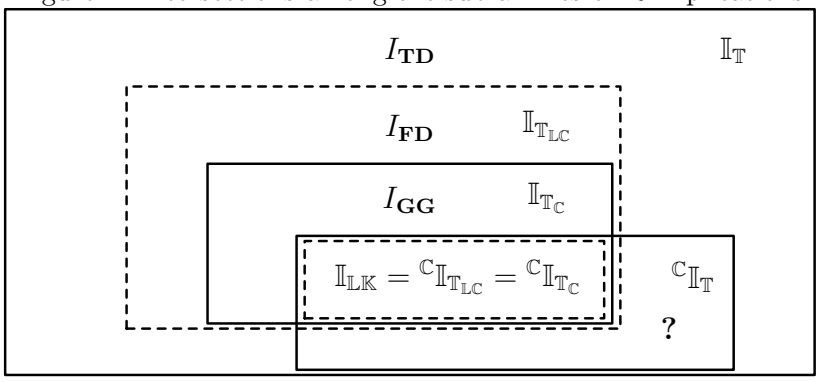

- $\mathbb{I}_{\mathbb{N}_\mathbb{T}(\mathbb{T}),\mathbb{N}_\mathbb{T}}$ is the family of all (S, N)-implications obtained from the N_T-dual t-conorms of the left-continuous t-norm T whose natural negation N_T is strong.

Theorem 10. *For a left-continuous t-norm T and a t-conorm S the following statements are equivalent:*

(i) The R-implication I_T is also an (S, N)-implication $I_{S,N}$.

(ii) The R-implication I_T is also an S-implication I_{S,N_T} with the strong negation N_T.

(iii) (T, N_T, S) form a De Morgan triple.

Remark 5. *The left-continuity of T is very important in the above theorem. For example, consider any t-conorm S whose natural negation $N_S \neq N_{\mathbf{D2}}$. However, $I_{S,N_{\mathbf{D2}}} = I_{\mathbf{TD}}$ which is also an R-implication obtained from the non-left-continuous t-norm $T_{\mathbf{D}}$. It is obvious that the triple $(T_{\mathbf{D}}, N_{\mathbf{D2}}, S)$ does not form a De Morgan triple.*

The results presented in this section are also diagrammatically represented in Figure 3.

7 Concluding remarks

From this discussion we see that the following open problems remain:

Problem 1. *Characterize the following:*

(i) (S, N)-implications generated from non-continuous negations;

(ii) R-implications generated from non-left-continuous t-norms;

Figure 3: Intersections between families of (S, N)- and R-implications

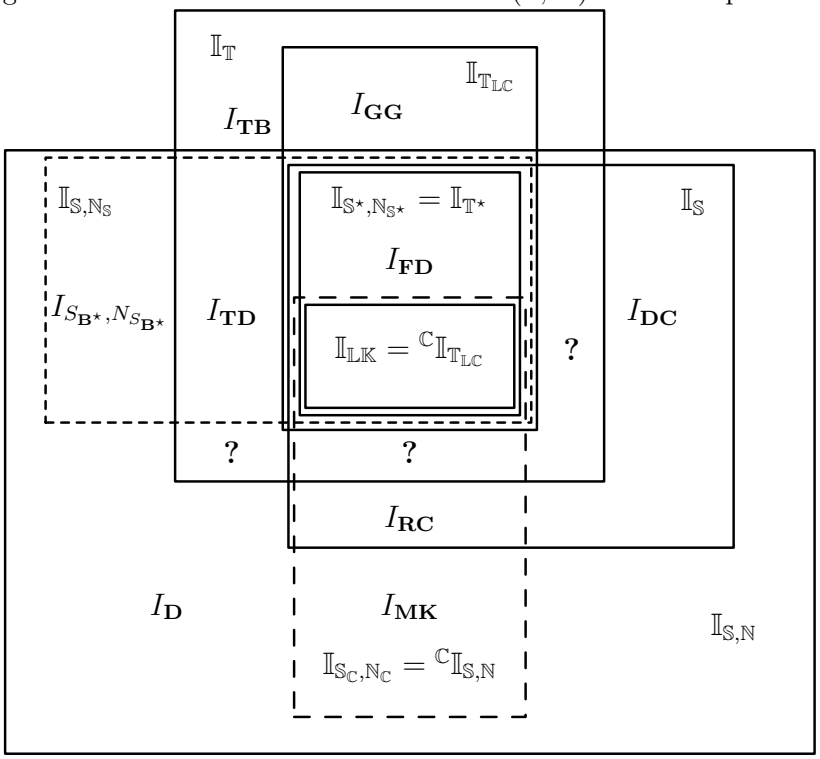

(iii) continuous R-implications generated from non-left-continuous t-norms;

(iv) the non-empty intersection $\mathbb{I}_{\mathbb{S},\mathbb{N}} \cap \mathbb{I}_{\mathbb{T}}$.

Acknowledgements

Part of this work was done when the author was a visiting researcher at the Faculty of Civil Engg., STU, Bratislava, for which he gratefully acknowledges the grant from SAIA that made this visit possible.

References

[1] M. Baczyński, Residual implications revisited. Notes on the Smets-Magrez Theorem, Fuzzy Sets and Systems 145 (2004) 267-277.

[2] M. Baczyński, B. Jayaram, On the characterizations of (S, N)-implications, Fuzzy Sets and Systems 158 (2007) 1713-1727.

[3] M. Baczyński, B. Jayaram, (S, N)- and R-implications: a state-of-the-art survey Fuzzy Sets and Systems, *In Press.*

[4] D. Dubois, H. Prade, A theorem on implication functions defined from triangular norms, Stochastica 8 (1984) 267-279.

[5] J.C. Fodor, M. Roubens, Fuzzy preference modeling and multicriteria decision support, Kluwer, Dordrecht, 1994.

[6] S. Gottwald, A treatise on many-valued logic, Research Studies Press, Baldock, 2001.

[7] M. Miyakoshi, M. Shimbo, Solutions of composite fuzzy relational equations with triangular norms, Fuzzy Sets and Systems 16 (1985) 53-63.

[8] P. Smets, P. Magrez, Implication in fuzzy logic, Internat. J. Approx. Reason. 1 (1987) 327-347.

[9] E. Trillas, L. Valverde, On implication and indistinguishability in the setting of fuzzy logic, in: J. Kacprzyk, R.R. Yager (Eds.), Management decision support systems using fuzzy sets and possibility theory, TÜV-Rhineland, Cologne, 1985, pp. 198-212.